Analysis of Microtubule Guidance in Open Microfabricated Channels Coated with the Motor Protein Kinesin†

John Clemmens,‡ Henry Hess,‡ Jonathon Howard,§ and Viola Vogel*,‡

Center for Nanotechnology and Department of Bioengineering, University of Washington, Seattle, Washington 98195, and Max Planck Institute of Molecular Cell Biology and Genetics, 01307 Dresden, Germany

Received June 28, 2002

Motor proteins such as kinesin are used in cells to transport intracellular cargo along defined filament paths. The constituents of the transport system (i.e., motor proteins and filaments) can be reconstructed on synthetic surfaces to serve as molecular shuttles that actively transport cargo. Microfabricated open channels have been used in the past to guide microtubules propelled by kinesin adsorbed to the surface. In an effort to better understand the mechanism by which guidance occurs, we present a quantitative measure of the transport efficiency of microtubules along straight polyurethane channels 1 μm deep. Our analysis shows that the probability of a microtubule remaining in a channel drops exponentially as a function of its travel distance and that this characteristic decay distance varies with channel width. We identify microtubule−sidewall collisions as the key event for microtubule escape from a channel and thus the determinant of guiding efficiency. To better understand the relationship between collisions and travel distance, we determine the effect of channel width on (1) the microtubule approach angle to the sidewall, (2) the collision outcome (guided or escaped), and (3) the distance traveled between collisions. Also discussed is how the physical properties of microtubules or actin filaments (i.e., length, bending stiffness, persistence length) and changes in channel geometry (width, height) can describe measured parameters.

Introduction

Directed transport of molecules and nanometer-sized cargo is an emerging challenge in nanotechnology. As complex synthetic devices shrink to cellular dimensions, active transport of nanocargo will be essential for direct molecular assembling, sorting, and sensing. In cells such processes are driven by motor proteins that convert the chemical energy of ATP hydrolysis into mechanical work to drive active transport along microtubules or actin filaments. By integrating motor proteins into synthetic devices, one can assemble a shuttle system where nanoscale cargo is moved between user-defined locations and against concentration gradients.[1] Designing efficient tracks for transport is a critical step in developing such molecular shuttle systems.

In this shuttle system tracks for motor proteins are derived from standard motility assays, where filaments such as microtubules[2] or actin[3] glide randomly on motor-protein-coated flat surfaces. Guiding of the filaments[4−10] has been achieved by patterning the surface with (a) a chemical pattern to selectively adsorb the motor proteins, (b) a topographical pattern to create guiding channels, or (c) a combination of selective adsorption and guiding channels. In previous studies the quality of guiding either was not quantified at all[4−8] or was assessed by measuring the distribution of filament orientations.[9,10] While the alignment of filament orientations parallel to the pattern of tracks presents evidence for guiding, it does not provide us with the information necessary to improve the engineering of tracks. Surface topography in straight microchannels of poly(methyl methacrylate)[6] and polyurethane[4] has been previously shown to guide filaments on myosin- and kinesin-coated surfaces, respectively. Our previous work[4] demonstrated that channels in polyurethane could guide microtubules through collisions with side walls. Microtubules traveling perpendicular to grooves frequently hit walls that disrupt movement by bending or detaching filaments.[4] Microtubules moving in the direction of the channels are able to glide without encountering walls, or are guided along the wall's edge after contacting the wall.

By changing the channel geometry (such as width or wall height), one may be able to increase the distance traveled by microtubules by decreasing the frequency of wall collisions or by increasing the number of guided microtubules in collisions. While the effect of wall height has already been studied,[11] we hypothesize that the frequency of collisions will be affected by the width of the channel. Furthermore, how they are affected will depend on physical properties that describe microtubule bending and movement on surfaces. Understanding how

* To whom correspondence may be addressed: tel, 206-543-1776; fax, 206-685-4434; e-mail, vvogel@u.washington.edu.

† Part of the *Langmuir* special issue entitled The Biomolecular Interface.

‡ University of Washington.

§ Max Planck Institute of Molecular Cell Biology and Genetics.

(1) Hess, H.; Vogel, V. *Rev. Mol. Biotechnol.* **2001**, *82*, 67−85.

(2) Howard, J.; Hunt, A. J.; Baek, S. *Methods Cell Biol.* **1993**, *39*, 137−47.

(3) Kron, S. J.; Toyoshima, Y. Y.; Uyeda, T. Q.; Spudich, J. A. *Methods Enzymol.* **1991**, *196*, 399−416.

(4) Hess, H.; Clemmens, J.; Qin, D.; Howard, J.; Vogel, V. *Nano Lett.* **2001**, *1*, 235−239.

(5) Hiratsuka, Y.; Tada, T.; Oiwa, K.; Kanayama, T.; Uyeda, T. Q. *Biophys. J.* **2001**, *81*, 1555−61.

(6) Riveline, D.; Ott, A.; Julicher, F.; Winkelmann, D. A.; Cardoso, O.; Lacapere, J. J.; Magnusdottir, S.; Viovy, J. L.; Gorre-Talini, L.; Prost, J. *Eur. Biophys. J.* **1998**, *27*, 403−8.

(7) Suzuki, H.; Oiwa, K.; Yamada, A.; Sakakibara, H.; Nakayama, H.; Mashiko, S. *Jpn. J. Appl. Phys., Part 1* **1995**, *34*, 3937−3941.

(8) Suzuki, H.; Yamada, A.; Oiwa, K.; Nakayama, H.; Mashiko, S. *Biophys. J.* **1997**, *72*, 1997−2001.

(9) Dennis, J. R.; Howard, J.; Vogel, V. *Nanotechnology* **1999**, *10*, 232−236.

(10) Nicolau, D. V.; Suzuki, H.; Mashiko, S.; Taguchi, T.; Yoshikawa, S. *Biophys. J.* **1999**, *77*, 1126−34.

(11) Stracke, P.; Bohm, K. J.; Burgold, J.; Schacht, H. J.; Unger, E. *Nanotechnology* **2000**, *11*, 52−6.

10.1021/la026155x CCC: $25.00
Published on Web 00/00/0000 PAGE EST: 6.8

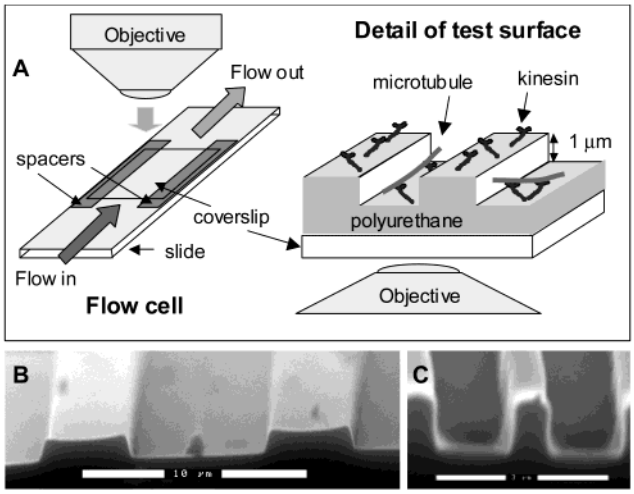

Figure 1. (A) Experimental setup of flow cells and polyurethane test surfaces mounted on coverglass. Scanning electron microscopy images of polyurethane channels of (B) 5.5 μm width and (C) 1.5 μm width. Particles observed in B are residue from the cross-sectioning procedure. Scale bars are (B) 10 μm and (C) 3 μm.

channel width and microtubule properties affect the frequency and guiding probability of wall collision events will help us to optimize the design of the tracks for molecular shuttles.

Materials and Methods

Kinesin Preparation. Expression of the wild-type *D. melanogaster* conventional kinesin gene construct with a histidine C-terminal tag and its purification by Ni^{2+} affinity column is described elsewhere.[12]

Preparation of Polyurethane Imprints. Our microfabricated patterns consisted of single isolated walls and open rectangular channels of various widths and single isolated walls. Replica molding[13] was used to imprint topography features into polyurethane with high fidelity. Briefly, a silicon wafer was coated with SU8-2 photoresist (MicroChem Corp., Newton, MA) and then exposed and developed to form a patterned photoresist on silicon. This surface was imprinted into poly(dimethylsiloxane) (PDMS; Dow Chemical, Midland, MI) and cured. Finally PDMS was imprinted a second time into polyurethane (NOA 73, Norland Products, Cranbury, NJ) with a cover glass backing (Corning) for support and was cured with ultraviolet light. The resulting surface replicated the patterned silicon surface with chemically uniform polyurethane. In preliminary tests, we found that the guiding probability was sensitive to the wall steepness produced by the imprinting technique. Scanning electron microscopy images revealed reduced wall steepness and rounded edges on the top and bottom of the walls in the polyurethane imprints after the stamp had been used for several months. Therefore we discarded stamps after five imprints or 2 months of use and used polyurethane imprints within 2 weeks. From electron microscopy, the steepness of polyurethane walls and sidewalls was verified to be ~80° as shown in Figure 1, parts B and C. For each channel width a minimum of 100 microtubules were analyzed from at least four separate channels and at least two surface preparations.

Motility Assay. Flow cells (Figure 1A) were assembled by sandwiching spacers[14] between the polyurethane film and a glass slide (Fisher Scientific, Pittsburgh, PA). The buffer for all experiments was BRB80 (80 mM Pipes, 2 mM $MgCl_2$, 1 mM EGTA, pH 6.85 with KOH). The flow cells were sequentially filled with a casein solution (0.5 mg/mL casein in BRB80), a conventional kinesin solution (~40 μg/mL kinesin with 0.2 mg/mL casein and 1 mM ATP in BRB80), and finally a motility solution (~3.2 μg/mL tetramethylrhodamine labeled microtubules (1−10 μm in length) containing 1 mM ATP and stabilized by 10 μM Taxol with oxygen scavenging additives (20 mM D-glucose, 20 μg/mL glucose oxidase, 8 μg/mL catalase, 0.2% 2-mercaptoethanol)). Flow cells were sealed with immersion oil to prevent evaporation. The assays were performed at room temperature (22 °C). Microtubules were visualized on the patterned surface by a Leica DM-IRBE fluorescent microscope (Leica AG, Wetzlar, Germany) using rhodamine filters. Topographic walls on the surfaces were simultaneously visualized by brightfield microscopy. For each region, sequential images of microtubules gliding along the surface were captured using a cooled-CCD camera (Orca2, Hamamatsu Photonics, Hamamatsu, Japan) with an imaged area of 64 × 80 μm. Microtubule positions were tracked with Metamorph image analysis software (Universal Imaging, Downingtown, PA).

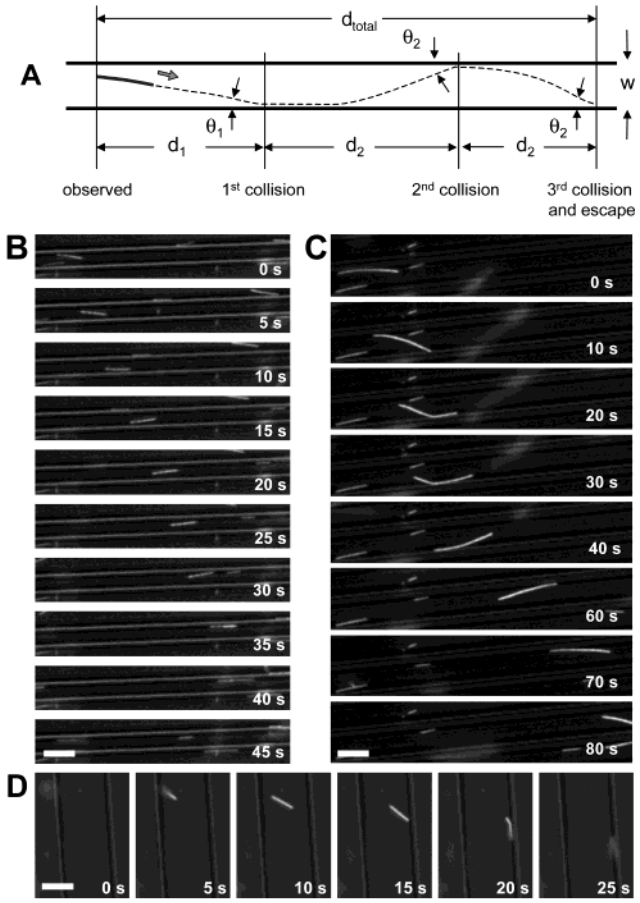

Figure 2. Measured parameters in microtubule guiding (A) and typical microtubule paths (B−D). (A) Measured parameters are channel width (w), the approach angles for first sidewall collision (θ_1) and subsequent sidewall collisions (θ_2), distance from observation to first sidewall collision (d_1), distance between sidewall collisions (d_2), and total distance traveled by the microtubule from first observation to escape (d_{total}). (B) Sequential images of a single microtubule on a 1.5 μm wide channel of polyurethane showing a path similar to that traced in (A). After landing (0 s), the microtubule is guided in its first sidewall collision (10 s) and then escapes out of focus in its second sidewall collision (40 s). (C) On a 2.5 μm wide channel, a microtubule lands (0 s) and is guided in two sidewall collisions (20 and 60 s) before moving off the screen. (D) On 5.5 μm channels we see a microtubule land (5 s) and collide with the sidewall at a large angle resulting in detachment from the surface (25 s). Scale bar is 4 μm for all image sequences.

Loss Rate Analysis. Microtubules were tracked as they glided along channels of different widths on the test surfaces. As a measure of how well each channel transported microtubules, we recorded the total distance traveled by the microtubule (d_{total}) in the channel (see results, Figure 2A). To understand how intermediate events such as wall collisions are influenced by

(12) Coy, D. L.; Wagenbach, M.; Howard, J. *J. Biol. Chem.* **1999**, *274*, 3667−71.
(13) Xia, Y. N.; Rogers, J. A.; Paul, K. E.; Whitesides, G. M. *Chem. Rev.* **1999**, *99*, 1823−1848.
(14) Limberis, L.; Stewart, R. J. *Nano Lett.* **2001**, *1*, 277−280.

channel width, the detailed analysis included measurements of the distance between first observation, collision events, and last observation before escaping the channel or moving from the field of view as shown in Figure 2A. "First observation" required a microtubule that landed or traveled from off the field of view to be completely in focus and within the bottom surface of the channels with both endpoints in the field of view.

A collision event could have two outcomes, guiding or escaping. A "guiding" event, as defined here, occurred if the microtubule aligned itself with the sidewall and remained traveling on the bottom of the channel. Microtubules that detached from the surface after hitting the sidewall or climbed up the wall were considered "escaped", or nonguided events. To ensure reliable measurements for guiding, the microtubules that slowly crawled up the sidewall and moved out of focus within 10 μm of the collision were counted as escaped. For consistency we recorded the collision point as the microtubule position (leading tip) one frame before bending or changing direction was clearly seen in the microtubule (point of collision counted in panels Figure 2B at 5 and 30 s, Figure 2C at 10 and 60 s, and Figure 2D at 15 s). A microtubule traveling along a wall will certainly experience many small collisions with the wall due to microtubule tip fluctuations. However, we could not resolve the fluctuations nor the small collisions, because these occurred at short time scales and/or over small distances. Therefore, we did not count additional collisions as the microtubule traveled along the wall, unless we could clearly distinguish another collision with the same wall, i.e., the microtubule traveled at least 0.5 μm away from the wall and then moved toward the same wall for another collision. Furthermore, microtubules were also considered to have escaped if they were stuck at the wall for more than 30 s (<5% of microtubules observed).

To measure the probability that a microtubule will travel a given distance, we first divided up the distance traveled by microtubules into 10 μm wide intervals. Based on these measurements, we calculated the probability $P_{\mathrm{loss},i}$ that a microtubule would escape the channel on the ith interval by $P_{\mathrm{loss},i} = N_{\mathrm{escape},i}/(N_{\mathrm{escape},i} + N_{\mathrm{remain},i})$, where $N_{\mathrm{escape},i}$ is the number of microtubules escaping on the ith interval and $N_{\mathrm{remain},i}$ is the remaining number of microtubules that do not escape but travel past that interval. The probability $P_{\mathrm{retained},i}$ that a microtubule would still be traveling after the ith 10 μm interval is related to $P_{\mathrm{loss},i}$ by

$$P_{\mathrm{retained},i} = (1 - P_{\mathrm{loss},i})P_{\mathrm{retained},i-1} \quad (1)$$

where $P_{\mathrm{retained},0} = 1$. Standard errors (SE) were determined for the probabilities by the formula

$$\mathrm{SE} = \left(\frac{P_{\mathrm{retained},i}(1 - P_{\mathrm{retained},i})}{N_{\mathrm{escape}.i} + N_{\mathrm{remain},i}}\right)^{1/2} \quad (2)$$

The histogram was fit to the equation $y = \exp(-x/x_0)$ weighted by standard errors, where x_0 is the fit parameter and characteristic decay length. The standard deviation for the fit parameter x_0 was also calculated in the analysis.

Approach Angle Analysis. Image analysis consisted of measuring coordinates for the topographical boundary (wall or channel sidewalls) and the endpoints of the microtubules as they approached that boundary. The microtubule coordinates were used to calculate an approach angle relative to the boundary: θ for a single wall (Figure 3B), or θ_1 and θ_2 for channels (Figure 2A). With the guiding and escaping events recorded for each collision, the approach angles were sorted into a histogram with 10° bin width. For each bin, the probability of guiding was calculated as the ratio of guided events divided by the total number of microtubules hitting the boundary in that bin. Standard errors were determined for the probabilities by the formula $\mathrm{SE} = (p(1-p)/N)^{0.5}$, where p is the probability of guiding for the bin and N is the total number of microtubules colliding in the bin.

Results

Channels with 1 μm high sidewalls and widths of 1.5, 2.5, or 5.5 μm were tested for their ability to guide microtubules. Microtubules in the channel were typically first observed after landing in the middle of the channel, crawling into the channel via the sidewall, or entering from outside the field of view. Microtubules traveled a distance measured as d_{total} before escaping the channel in wall collisions, typically by crawling up or over the sidewall, or detaching completely from the surface. Measurements of d_{total} were used to compute the probability that a microtubule would reach a certain distance in the channel before escaping. Shown in Figure 4, these probabilities decay exponentially to the equation $y = \exp(-x/x_0)$. The characteristic travel length x_0 is the distance that a fraction of microtubules equal to $1/e$ (~37%) remain traveling in the channel. From least-square fits to the data in Figure 4 with standard errors as weighting factors, we obtained x_0 values of 26.4 ± 2.4, 34.5 ± 3.2, and 26.6 ± 2.0 μm (mean ± standard error), for 5.5, 2.5, and 1.5 μm wide channels, respectively. Assuming x_0 follows a normal distribution, its mean for 2.5 μm wide channels is marginally different than x_0 for 1.5 or 5.5 μm wide channels ($p \approx 0.05$).

We confirmed that the difference between x_0 values was not due to a difference in average microtubule length. By

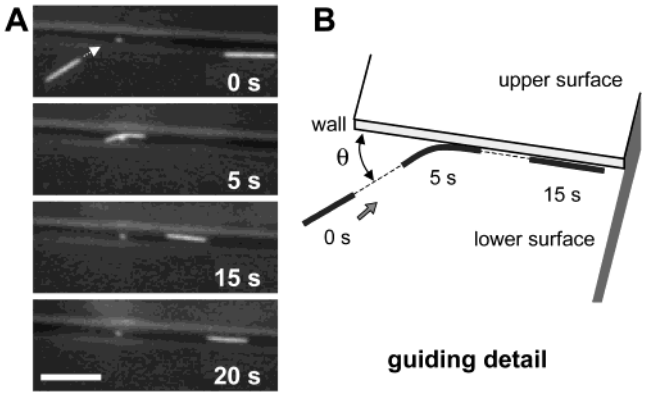

Figure 3. Measured parameters in microtubule guiding by a single wall. (A) Sequential images of a microtubule as it is guided by a 1 μm high wall of polyurethane (5 s intervals). The microtubule bends as it hits the wall (5 s) and aligns to the wall direction (15 and 20 s) while continuing to be transported along the bottom surface. Scale bar is 4 μm. (B) Schematic illustrating measured parameters in the guiding example in (A). The approach angle θ and collision outcome (guided or escaped) are recorded.

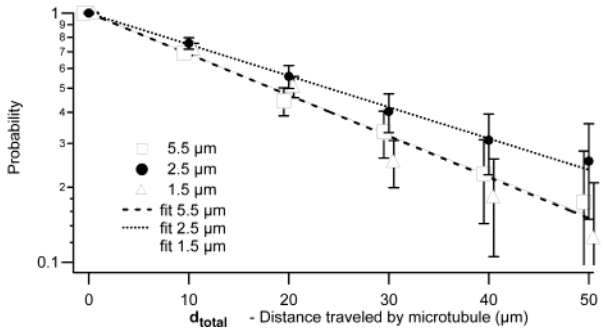

Figure 4. Probability of microtubules traveling a given distance d_{total} before escaping on 1.5, 2.5, and 5.5 μm wide channels. Probabilities ± standard errors are shown and are least-squares fit to $y = \exp(-x/x_0)$ with x_0 = 26.4 ± 2.4, 34.5 ± 3.2, and 26.6 ± 2.0 μm (mean ± standard error) for the 5.5, 2.5, and 1.5 μm wide channels, respectively. The mean x_0 for 2.5 μm wide channels was larger than that for 1.5 μm wide channels ($Z = 2.03$; $p = 0.04$) and 5.5 μm wide channels ($Z = 2.09$; $p = 0.04$). There was no difference between mean x_0 for 1.5 and 5.5 μm wide channels ($Z = 0.06$; $p = 0.95$).

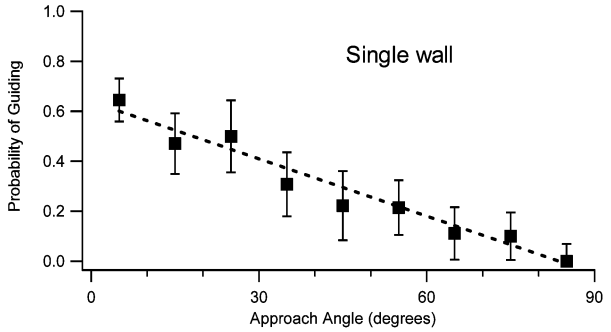

Figure 5. Probability of microtubule guiding for various approach angles, θ, to a 1 μm high single wall of polyurethane ($\pm$standard error). A linear fit of the data is represented by the dashed line $y = 0.64 - 0.0076x$. Average microtubule length is 4.4 $\pm$ 2.9 μm (mean $\pm$ standard deviation). (N = 128 total collisions, bin width = 10°.)

including only lengths between 1 and 5 μm, our analysis held microtubule length constant between channels with average lengths of 2.9 $\pm$ 0.9, 3.2 $\pm$ 0.9, and 3.0 $\pm$ 0.8 μm (mean $\pm$ standard deviation), for 5.5, 2.5, and 1.5 μm wide channels, respectively.

For the channels tested we noted that microtubules often experienced consecutive collisions on opposite walls before detachment. If microtubules always had the same probability of being lost over the wall or detaching on each collision, one would expect the widest channels to have the largest d_{total} values—and thus the largest x_0 values—due to the additional travel length to cover the increased spacing between walls. Figure 4, however, does not show increasing x_0 for wider channels. This prompted us to study in more detail how the effect of wall collisions and the distances between collisions are influenced by channel width. Our detailed measurements are sketched in Figure 2A.

First, we studied the probability of microtubule guiding during collisions with single 1 μm high walls in more detail (Figure 3). In agreement with previous findings,[4,5] walls could guide microtubules by bending the microtubule's leading tip into alignment with the wall (Figure 3A, 5 s). Microtubules approaching at shallow angles (small θ) were frequently guided by slight bending, while collisions at larger angles rarely resulted in guiding (Figure 5). For microtubules traveling along the edge of the wall, two paths are possible because all surfaces are coated with kinesin. Those paths are (1) climbing up the wall (escaping) and (2) traveling along the bottom surface (guiding). Each of these paths is equally possible at shallow approach angles as shown by ~50% probability of guiding. In all cases the amount of microtubule bending at wall collisions was considerably greater than for microtubules gliding on flat surfaces. We therefore conclude that additional microtubule bending at walls is a result of kinesin pushing the microtubule against the wall, similar to microtubule buckling experiments.[15]

Second, we studied microtubules traveling in channels in more detail. Once landing in the middle of the channel or crawling into the channel via the sidewalls, microtubules traveled a distance measured as d_1 before first contacting the wall. As shown in Table 1, the microtubules traveled an average d_1 of 12 $\pm$ 10, 14 $\pm$ 10, and 12 $\pm$ 7 μm (mean $\pm$ standard deviation) for channels widths of 5.5, 2.5, and 1.5 μm, respectively.

After landing and traveling d_1, the first collision with the wall at angle θ_1 was different for each width of the channel as indicated by the average values in Table 1. While microtubules approached the single wall at all angles nearly equally (data not shown), the approach angle was distributed more closely around smaller angles as the width of the channel decreased. Consequently, we measured average θ_1 values of 37 $\pm$ 22°, 20 $\pm$ 11°, and 15 $\pm$ 11° (mean $\pm$ standard deviation) for 5.5, 2.5, and 1.5 μm wide channels, respectively (Table 1).

One possible explanation for shallower approach angles in narrower channels is that as the width decreases below the microtubule length, microtubules must be nearly aligned with the channel to move along the bottom of the channel. This implies that longer microtubules would be better aligned to the channel and would collide with smaller θ_1 on average. To check for a correlation between microtubule length and approach angle range, we recalculated the range of θ_1 including microtubules with lengths over 5 μm (data not shown). We found an increase in the number of events at shallow approach angles suggesting that longer microtubules contributed to those events, consistent with our explanation.

To account for our measured ranges for θ_1, we estimate the largest possible approach angle that occurs when the microtubule spans the width of the channels with ends at opposing sidewalls. We estimate the largest possible approach angle θ_1 as

$$\max \theta_1 \approx \arcsin(w/L_{MT}) \qquad (3)$$

where w and L_{MT} are channel width and microtubule length, respectively. For a 1.5 μm channel and an average microtubule length of 3.0 μm, we estimate max $\theta_1 \approx$ arcsin(1.5 μm/3.0 μm) = 30°. Assuming θ_1 is uniformly distributed between 0° and 30°, we estimate mean $\theta_1 \approx$ 15°, which agrees with measured θ_1 = 15° (Table 1). For 2.5 μm wide channels, we calculate a max θ_1 = arcsin(2.5 μm/3.2 μm) $\approx$ 51° and estimate a mean $\theta_1 \approx$ 21°, which compares well with measured θ_1 = 20°. For 5.5 μm wide channels, microtubules had a mean length of 2.9 $\pm$ 0.9 μm and were short enough to stretch across the width of the channel without contacting sidewalls. In this case the estimated mean $\theta_1 \approx$ 45°, larger than the measured value of 37° (Table 1), can be attributed to the fact that the θ_1 was not equally distributed and had only a few collisions orthogonal to the wall.

After a first collision, guided microtubules moved along a channel to their next collision. The distances between subsequent collisions d_2 were longer than distances from landing to the first collision d_1 and were 24 $\pm$ 14, 17.0 $\pm$ 8, and 16.6 $\pm$ 7 μm (mean $\pm$ standard deviation), for channel widths of 5.5, 2.5, and 1.5 μm, respectively (arrows in Figure 6). The collision distance d_2 for 5.5 μm wide channels was larger than for 1.5 or 2.5 μm wide channels (Figure 6). This might be accounted for by the fact that when walls are close together as in narrower channels, an aligned microtubule need not deviate far from a straight path to cause a second collision. For wider channels, longer distances must be covered by a microtubule before it deviates far enough to collide with the opposite wall.

The angle of subsequent collisions (θ_2) also increased with increasing channel width as shown in Figure 7, where we noted a consistent decrease in mean θ_2 compared to mean θ_1. The average subsequent collision angle θ_2 was 28 $\pm$ 22°, 17 $\pm$ 10°, and 11 $\pm$ 7° for 5.5, 2.5, and 1.5 μm wide channels, respectively (Table 1).

Discussion

Our analysis found the probability of a microtubule remaining in a channel dropped exponentially as a function

(15) Gittes, F.; Meyhofer, E.; Baek, S.; Howard, J. *Biophys. J.* **1996**, *70*, 418−29.

Table 1. Summary of Measured and Predicted Values for Microtubules Traveling in Polyurethane Channels[a]

	5.5 μm wide channels		2.5 μm wide channels		1.5 μm wide channels		notes on predicted values
	measured	predicted	measured	predicted	measured	predicted	
d_1	13 ± 11 μm	<39 μm	12 ± 10 μm	<23 μm	11 ± 8 μm	<17 μm	see eq 8
θ_1	37 ± 22°	45°	20 ± 11°	21°	15 ± 11°	15°	see eq 3
d_2	24 ± 14 μm	39 μm	17.0 ± 8 μm	23 μm	16.6 ± 7 μm	17 μm	see eq 8
θ_2	28 ± 21°	16°	17° ± 9°	13°	11 ± 7°	10°	see eq 9
x_0	26.4 ± 2.4 μm	26 μm	34.5 ± 3.2 μm	28 μm	26.6 ± 2.0 μm	29 μm	see eq 11
L_{MT}	2.9 ± 0.9 μm		3.2 ± 0.9 μm		3.0 ± 0.8 μm		
$p_{guiding}$	0.38	0.36	0.59	0.49	0.50	0.52	from Figure 5

[a] All measured values are mean ± standard deviation. d_1, θ_1, d_2, and θ_2 are distances and angles shown in Figure 2A. x_0 is the characteristic decay length for travel distance (see Figure 4). L_{MT} is the microtubule length. $p_{guiding}$ is the guiding probability for microtubule−sidewall collision (see Discussion).

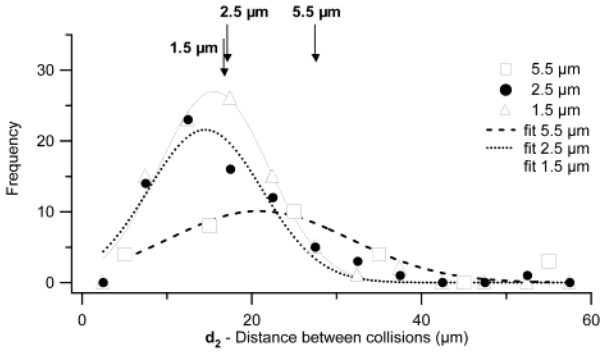

Figure 6. Distribution of distances between consecutive collision events, d_2, shown for 5.5 μm wide channels (squares), 2.5 μm wide channels (circles), and 1.5 μm wide channels (triangles). Mean values for d_2 are marked with an arrow at the top of the graph for each width. Lines show least-squares fit of a Gaussian curve to the distribution showing that d_2 shifts to larger distances for wider channels. (Bin width = 5 μm for 1.5 wide and 2.5 μm wide channels and = 10 μm for a 5.5 μm wide channel).

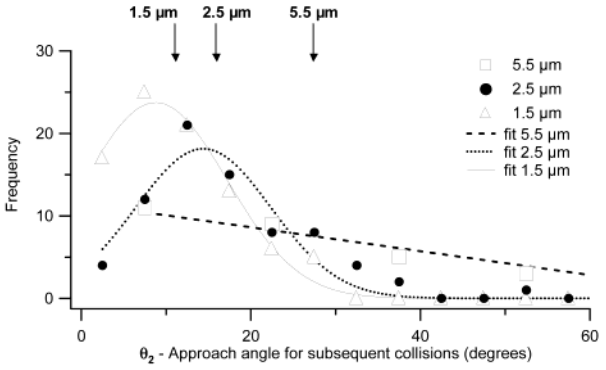

Figure 7. Distribution of microtubule approach angles for subsequent wall collisions, θ_2, shown for 5.5 μm wide channels (squares), 2.5 μm wide channels (circles), and 1.5 μm wide channels (triangles). Mean values for θ_2 are marked with an arrow at the top of the graph for each width. (Bin width = 5° for 1.5 and 2.5 μm and = 10° for 5.5 μm wide channels).

of its travel distance and the characteristic decay distance was marginally different between 2.5 μm channels and either 5.5 or 1.5 μm wide channels. Further, we identified microtubule−sidewall collisions as the key event for the escape of microtubules from a channel and thus the determinant of microtubule transport efficiency. To better understand the relationship between collisions and travel distance, we determined the effect of channel width on (1) the microtubule approach angle to the sidewall, (2) the collision outcome (guided or escaped), and (3) the distance traveled between collisions. To explain these results, we will discuss how the bending forces influence guiding by walls, how distance between collisions can be described by the persistence length, and how the average microtubule travel distance can be estimated from measured parameters.

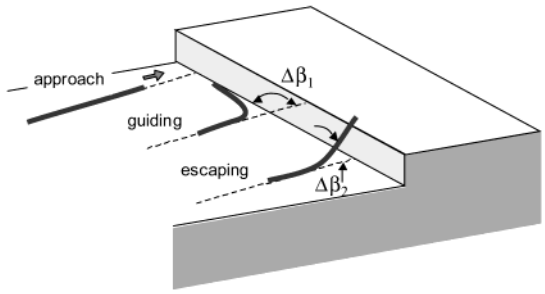

Figure 8. Possible paths for a microtubule approaching a wall at large angles (top) are to remain on the lower surface by guiding (center) or to reach the top surface by climbing the wall (bottom). The reduced bending angle and increased radius of bending from the approach path (dashed lines) may contribute to the escaping path being energetically favorable at large approach angles.

Bending Forces on Microtubules Predict Guiding Dependence on Approach Angle. In these experiments we confirmed that micrometer high walls can alter the paths of microtubules gliding on a surface.[11] While kinesin exerts forces on microtubules to propel them along the surface, walls act as rigid barriers that exert opposing forces to movement, causing microtubule bending[16] similar to that observed for anchored microtubules.[15] The bending energy E_b stored in the microtubule depends on the flexural rigidity EI ($\approx 30 \times 10^{-24}$ N m^2, ref 15) (where E and I are the modulus of elasticity and the moment of inertia, respectively), the radius of curvature of the bend r, and the bending angle $\Delta\beta$ and can be estimated as

$$E_b = {}^1/_2 EI \int_0^s \left(\frac{d\theta}{ds}\right)^2 ds = \frac{EI}{2r}\Delta\beta \qquad (4)$$

Therefore, the microtubule path of least bending angle and largest bending radius will be energetically favorable. We estimate the difference in energy between a guiding and an escaping microtubule in wall collisions as illustrated in Figure 8. From our observations it is difficult to accurately measure where microtubules actually detach while climbing walls. As a first approximation, we assume a microtubule of average length (L_{MT}) climbs the wall with its bent shape following a circular arc. We also assume the microtubule detaches at a distance of half of its length (~1.5 μm) from the intersection point of the approach path (Figure 8, dashed line) and the wall. With these assumptions, we calculate the angular dependence for the guiding path as

(16) Hess, H.; Clemmens, J.; Matzke, C. M.; Bachand, G. D.; Bunker, B. C.; Howard, J.; Vogel, V. *Appl. Phys. A: Mater. Sci. Process.* **2002**, *75*, 309−313.

$$E_b = \frac{EI\,\Delta\beta_1}{2r} = \frac{EI\,\Delta\beta_1}{2(L_{MT}/2)}\tan\left(\frac{\Delta\beta_1}{2}\right) \quad (5)$$

For a microtubule approaching perpendicular to the wall (Figure 8), we find that a guided microtubule must bend $\Delta\beta_1 = 90°$ to align along the wall, while the escaping path need only bend $\Delta\beta_2 \approx 67°$ to climb the 1 μm high wall. The radius of bending is larger in the escaping case ($\sim$1.6 μm) compared to the guided case (1.5 μm). Taken together in eq 4, the energy needed for the guided case is 46% ($\sim$800kT) greater than that needed for the escaping path at a 90° approach angle, thus favoring the escaping path energetically for large approach angles and accurately predicting the measured guiding probability of zero.

For shallow approach angles, the bending angle to align with the wall is very small and, by eqs 4 and 5, microtubules should always travel the "guided path", which in fact has a maximum guiding probability of $\sim$50% as discussed earlier in the results section. In the "guided path", the bending angle ($\Delta\beta_1$) for a microtubule can be approximated by the approach angle (θ_1 or θ_2), thus our calculations correctly predict the continuous decrease in probability as the approach angle increases and the escaping case becomes more favorable. However, our calculations estimate the "guided path" and "escaping path" to be equal energetically (corresponding to a guiding probability of $\sim$25%) at $\Delta\beta_1 = \Delta\beta_2 \approx 78°$ instead of the measured value of $\sim$45° (Figure 5). We may correct eq 5 at intermediate angles by including energies for kinesin binding to the "guided path" bending microtubule when more detailed measurements of microtubule/wall collisions are possible.

Persistence Length Predicts That Collision Distances Depend on Channel Width. While on flat surfaces and traveling over small distances, a microtubule glides more or less along a straight path in the absence of external forces. Over large distances (on the order of millimeters) the direction that a microtubule moves is not correlated with its initial direction. The persistence length relates how a microtubule's path will deviate from a straight segment or how the path is curved on average. Assuming a microtubule is aligned along one sidewall of the channel, we can estimate the average distance L traveled in the channel before colliding with the opposite sidewall. We can simplify our calculation by considering a rod that traces a circular arc beginning and ending on one sidewall at distance 2L apart and with its midpoint on the opposite sidewall. The average energy $\langle U\rangle$ stored in the rod can be written as

$$\langle U\rangle \approx EI\,\langle L/R^2\rangle = {}^1/_2 kT \quad (6)$$

where EI is the bending rigidity of the rod, R is the radius of circular path, and kT is the unit of thermal energy causing the bend. Geometrically, R is calculated from L and w by

$$R \approx L^2/2w \quad (7)$$

Substituting eq 6 into eq 7 with the 2-D persistence length[19] L_p given by $L_p = 2EI/kT$, the average distance traveled between collisions $\langle L\rangle$ relates to channel width w by

$$\langle L\rangle = (4w^2 L_p)^{1/3} \quad (8)$$

The corresponding approach angle α of the collision at the wall is

$$\alpha = \arcsin(2w/L) \approx \theta_2 \quad (9)$$

The persistence length of a microtubule path predicts the order of magnitude of the collision distances. Importantly, it predicts the wider the channel, the longer the collision distance, but the distance increases only as $w^{2/3}$. Instead of estimating a persistence length from a free microtubule in solution (2-D $L_p \approx 12$ mm (see ref 17)), we use a direct measurement of the persistence length of the microtubule path on a glass surface (2-D $L_p \approx 500$ μm), which will be reported elsewhere.[18] We estimate the distance between collisions $d_2 \approx \langle L\rangle = 39$, 23, and 17 μm for 5.5, 2.5, and 1.5 μm wide channels, respectively. This relationship agrees well with d_2 measured in 1.5 μm wide channels (16.6 μm), though overestimates the measured values of d_2 for 2.5 and 5.5 μm channels (Table 1). The corresponding estimated values for θ_2 are 16°, 13°, and 10° for 5.5, 2.5, and 1.5 μm wide channels, respectively, where values for 1.5 μm channels agree with the measure value of 11 $\pm$ 7°, and other estimates are increasingly lower than measured values as the increasing width. Because shorter distances correlate with larger approach angles in eq 9, the approach angle α will be underestimated when the distance is overestimated as observed.

Occasionally a microtubule would have consecutive collisions on the same sidewall rather than on the opposite sidewalls. This phenomenon may be responsible for estimated d_2 values greater than those measured, because the microtubule will travel a shorter distance than the width of the channel. We expect this to be more of a factor in wide channels than narrow channels because of our collision criteria.

Additionally, a discrepancy between measured and estimated values could arise from underestimating the true value of d_2 in 2.5 and 5.5 μm channels due to the limited area recorded from our microscope. Microtubules have already traveled $\sim$12 μm (mean d_1) before contacting the wall; thus microtubules traveling large d_2 distances and those landing in the middle of the field of view may travel off the screen (64 μm $\times$ 80 μm viewable area) before their second collision. Because microtubules land randomly along the length of each channel, the contribution of this effect is difficult to measure.

Calculating an exact collision distance for d_1 and angle θ_1 is complicated by the distribution of landing angles. The measured values of d_1 do not increase with width as predicted by eq 8 because wide channels have more broadly distributed landing angles and/or more frequently allow microtubules to land in the center of the channel. Thus, the microtubule path from landing to first collision (d_1) will be only a fraction of the path between opposite walls (d_2). Therefore, we estimate d_2 distances as an upper limit for measured d_1 values. The average measured d_1 is less than the estimated d_2 in all cases (Table 1). The variation in landing angles also makes θ_1 difficult to estimate with eq 9, which assumes microtubules start parallel with the channel sidewalls.

Our calculations using the persistence length of a microtubule path prove to be most accurate for microtubules that always curve to the opposite wall and start along the channel sidewall. To further refine predicted values, a more complex relation should be used that describes all observed paths of microtubules, including those with consecutive same-sidewall collisions, partial distances due to landing, and variable landing angles. The calculations also are only accurate for channels where

(17) Mickey, B.; Howard, J. *J. Cell Biol.* **1995**, *130*, 909−17.
(18) Hess, H.; Vogel, V. In preparation.

$w \ll L_p$. This intuitively makes sense as for wide channels microtubules will travel a far enough distance to reach the other wall that its direction and position will not be correlated with that from the prior collision, making travel distance and approach angle difficult to predict. Alternatively, paths of flexible filaments such as actin will be uncorrelated at even shorter traveling distances and even narrower channels. In related experiments[18] we found the persistence length of a microtubule path (2-D $L_p \approx 500$ μm) to be on the order of 24-fold smaller than microtubules free in solution (2-D $L_p \approx 12$ mm (see ref 17)) due to reasons still under investigation. Assuming that the persistence length for an actin path is less than the value measured for free actin in solution (2-D $L_p \approx 30$ μm (see refs 19 and 20)), the persistence length analysis may not be accurate for guiding assays of actin on myosin surfaces, where channel widths of a few micrometers and persistence lengths of an actin path are of the same order of magnitude.

Estimation of Average Travel Length x_0. To design channels that maximize the distance traveled by microtubules, we must consider two effects that vary with the width of channels: Increasing the width of channels will allow microtubules to travel longer distances between collisions (large values for d_2), yet decreasing the width ensures that collisions are at shallow approach angles and have an increased chance of being guided. We illustrate these effects by estimating average travel length x_0.

For each channel, the decay length x_0 from Figure 3 is also the mean distance $\langle d_{total} \rangle$ traveled by a microtubule. We can write $\langle d_{total} \rangle$ as a sum of the measured distances d_1 and d_2, where terms form a geometric series

$$\langle d_{total} \rangle = d_1(1 - p_{guiding}) + (d_1 + d_2)p_{guiding}(1 - p_{guiding}) + (d_1 + 2d_2)p_{guiding}^2(1 - p_{guiding}) + \ldots \quad (10)$$

$$\langle d_{total} \rangle = d_1 + d_2\left(\frac{p_{guiding}}{1 - p_{guiding}}\right) = x_0 \quad (11)$$

where $p_{guiding}$ is the average probability of guiding for all collisions in that width channel. Using measured values of $p_{guiding}$ from Table 1, we calculate an x_0 value and compare it to the measured values (shown in parentheses) with values of $x_0 = 27.6$ μm (26.4 $\pm$ 2.4 μm), 36.3 μm (34.5 $\pm$ 3.2 μm), and 27.3 μm (26.6 $\pm$ 2.0 μm) for 5.5, 2.5, and 1.5 μm wide channels, respectively. Assuming all sidewall collisions follow Figure 5, we can also estimate $p_{guiding}$ by the corresponding probability of the average approach angle θ_1 (Table 1). With this estimated value for $p_{guiding}$, the mean travel distance should be the same for all channels ($x_0 = 26$, 28, and 29 μm for 5.5, 2.5, and 1.5 μm wide channels, respectively). This suggests that the difference in travel distance (Figure 4) is due to a small, but detectable, increase in guiding in 2.5 μm wide channels (measured $p_{guiding} = 0.59$ vs predicted $p_{guiding} = 0.49$). Thus, this result suggests that channel sidewalls vary in their ability to guide microtubules. Because we measured the sidewall steepness to be the same in all channels, microtubule guiding may possibly be sensitive to topography changes that are below our resolution of measurement.

The significance of eq 11 in this example is that the distance traveled (or x_0 value) is very sensitive to the guiding probability. Future efforts to optimize microtubule tracks will prove most effective by increasing the guiding probability, either through modulating track geometry, as presented here for channel width, or through alternative fabrication strategies.[5]

Conclusion

This study provides the quantitative groundwork where for the first time both the physical properties of microtubules and shuttle track geometry (channel width) are evaluated in terms of their contribution to microtubule guiding on a topographically micropatterned surface. Both experimentally and theoretically, we found that decreasing channel width had canceling effects of (1) increasing the collision rate of microtubules with the sidewalls and (2) increasing the probability of guiding at collisions by changing the microtubule approach angle. Many of the derived relationships for guiding in polyurethane channels apply for other surface fabrication methods, and the steps used to develop the equations may even apply in other fields that analyze transport (e.g., a neurophysiologist finds key geometrical cytoskeleton arrangements that influence vesicle transport efficiency in cells). With the knowledge gained from this study, we can concentrate our efforts on improving guiding in shuttles with predictable advances for molecular shuttle transport. These advances to improve user-defined active transport will open the door for nanoscale devices powered by motor proteins.

Acknowledgment. We acknowledge Emilie Warner for helpful comments on the manuscript and Greg Golden for ESEM assistance. J.C. was supported in part by a fellowship from the Center of Nanotechnology (UIF) and National Science Foundation (Integrative Graduate Education and Research Training). H.H. was supported in part by the Alexander-von-Humboldt foundation. This work was funded by NASA Grant NAG5-8784.

LA026155X

(19) Gittes, F.; Mickey, B.; Nettleton, J.; Howard, J. *J. Cell Biol.* **1993**, *120*, 923−934.

(20) Yanagida, T.; Nakase, M.; Nishiyama, K.; Oosawa, F. *Nature* **1984**, *307*, 58−60.